BIOMASS P-band Interferometry: Temporal Stability Study and Comparison with Airborne SAR Experiments in Gabon.

Fred Terrance Ndouni Missono[a], Irena Hajnsek[a,b], Roman Guliaev[a], Konstantinos Papathanassiou[a]
[a]Microwaves and Radar Institute, German Aerospace Center, Germany
[b]ETH Zurich Institute of Environmental Engineering, Switzerland

Abstract

ESA's BIOMASS mission offers a unique opportunity to estimate aboveground forest biomass and to monitor forest dynamics on an almost global scale by means of interferometric and tomographic techniques. The long wavelength (P-band) combined with the three-day repeat-pass cycle enable high-quality interferograms. At the same time, the variable non-zero spatial baseline makes the P-band interferometric coherence intrinsically sensitive to the volumetric distribution of scatterers even in dense tropical forests, and, therefore, sensitive to forest height and structure. However, the interferometric coherence is also subject to temporal decorrelation. In this context, a new AfriSAR-3 airborne campaign, conducted in Gabon in November 2025 at the end of the BIOMASS in-orbit commissioning phase (IOC), aims to cross-validate the level of temporal decorrelation in the BIOMASS interferograms. This study conducts an in-depth analysis of the estimated temporal decorrelation levels using fully polarimetric and interferometric/tomographic airborne datasets and compare the results with those obtained from BIOMASS.

1 Introduction

Gabon's tropical forests, estimated to cover 89% of the country's territory [1] play a major role in the global carbon cycle and climate regulation, particularly in terrestrial carbon storage.
This is because Gabon's tropical forests are among the highest and most carbon-rich in the world, with average canopy heights of up to 50 m in the Mondah and La Lopé regions, and up to 60 m in the dense forests of the Mabounie region [2], as well as mangroves of up to 60 m in the Pongara region [3].

Estimates of above-ground biomass (AGB), based on pan-tropical biomass maps [4], indicate values generally ranging from 10 t.ha-¹ in savannah areas to 600 t.ha-¹ in dense forests [2]. Because of their vast extent and complex structure, Gabon's forests are a critical element in climate regulation and the global carbon cycle.

The BIOMASS mission, launched in April 2025 by the European Space Agency (ESA), the estimation of forest height and biomass, and the detection of forest disturbances. Its fully polarimetric P-band radar, operating with a three-day repeat-pass interferometric cycle, provides a rich dataset to achieve these objectives. The long wavelength (approximately 70 cm) ensures sufficient penetration and allows for the observation of structural properties even in the densest tropical forests, such as those in Gabon.

However, the interferometric coherence is also affected by temporal decorrelation, which can arise from wind-induced motion or dielectric changes within the scattering volume. Additionally, signal propagation through the ionosphere requires specific calibration and correction steps, which can further complicate the interpretation of temporal variations in the radar backscatter.

In this context and in the frame of the BIOMASS Cal-Val activities, the AfriSAR-3 airborne campaign was conducted in Gabon in November 2025, at the end of BIOMASS in-orbit commissioning phase. The campaign data will allow to assess, across other issues, the temporal stability of P-band radar coherence during the BIOMASS acquisition, matching the temporal and interferometric baselines of BIOMASS.

This study therefore aims to quantify, model and interpret the temporal decorrelation of the P-band radar signal using fully polarimetric and interferometric/tomographic airborne datasets and compare it to the one of BIOMASS. In addition, the long-term temporal coherence of several months and years will be assessed based on the previous AfriSAR-1/-2 campaigns in 2016 and 2023.

2 Airborne campaigns

The data used in this study are from the AfriSAR-3 (GABONX-2) campaign performed in November 2025 in Gabon, with the acquisition of fully polarimetric P-band tomographic data by DLR's F-SAR airborne sensor [5] in the same configuration as AfriSAR-1 2016 and AfriSAR-2 2023 [6] in zero baseline configuration. The main test sites were La Lopé, Mabounie, Mitzic, Ipassa (Makokou), Pongara and Mondah. To facilitate direct comparison between airborne and BIOMASS measurements, the heading direction and mean incidence angle of the F-SAR were aligned with those of BIOMASS.

The acquisitions of AfriSAR-3 were planned simultaneously with the BIOMASS acquisitions, and the temporal and spatial interferometric baselines also match the BIOMASS configuration. In addition, date acquired in the frame of the two previous AfriSAR campaigns performed in 2016 and 2023 are analysed for long-term coherence of tropical forests in Gabon over several months

and years. Finally, BIOMASS acquisitions in the zero-base configuration of Commissioning Phase 1 (COM-1) are analysed. These data were acquired in June 2025, 09.06.25, 12.06.25 and 15.06.25, i.e. three of the six days of the baseline and one of the 9 days acquired in May.

3 Study area

Our study is performed at the Mondah and La Lopé pilot sites in Gabon (Figure 1).
Mondah is located in the northwest of Gabon. The western part contains a primary forest over 50 m high in the Raponda Walker Arboretum, with dense, homogeneous stands, while the eastern part is covered with secondary forest [7]. The topography is relatively flat. This is a region that is increasingly affected by deforestation, due to urban expansion and the development of socio-economic activities such as agriculture, sand and soil extraction, etc. It has a typically equatorial climate, with fairly abundant rainfall for 9 months of the year (September - May), an average of 1,800 mm/year and an average temperature of 28°C.

The La Lopé site is located in the Lopé National Park in central Gabon. It contains a variety of forest structure types, ranging from open savannahs with sparse mixed forest stands to dense, undisturbed and large (sometimes exceeding 50 m) stands of monodominant Okoumé (characteristic of dense, single-layered, tall and dense forest stands) [8],[9],[10]. The site's relief is marked by numerous local slopes in excess of 20°.

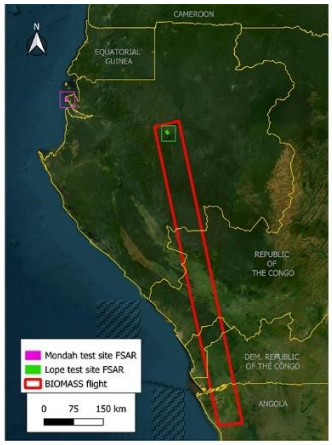

Figure 1: Location of the study area

4 Results

4.1 Airborne temporal stability

The temporal stability of the P-band radar signatures between 2016 (AfriSAR), 2023 and 2025 (GabonX) is evaluated by calculating the interferometric coherence (1) [11] in HH polarisations between two successive acquisitions by varying the temporal baseline, first for 3-4 days and then for 7-8 days for each of the missions so as to be superimposable on the temporal resolution of the BIOMASS satellite. The interferometric coherence is given as:

$$\tilde{\gamma}(\vec{w}) = \frac{<S_1(\vec{w})S_2^*(\vec{w})>}{\sqrt{<S_1(\vec{w})S_1^*(\vec{w})><S_2(\vec{w})S_2^*(\vec{w})>} \qquad (1)$$

with $0<\gamma<1$, S_1 and S_2 represent images 1 and 2 respectively from each of the two successive flights acquired in the same flight configurations and $\vec{w}$ is the unitary complex vector related to the choice of polarization.

In the following only "zero spatial baseline" interferograms and coherences are discussed. The interferometric coherence between flights FL02 and FL05 (Figure 2 left) of AfriSAR-2 2023 in HH polarisation after three days remains relatively stable and high with an average level of 0.74 (Figure 3). However, the interferometric coherences between two flights separated by four days, FL05 and FL10 (Figure 2 middle), and FL05 and FL11 (Figure 2 right) show a slight drop in coherence from one to the other.

The two flights were made on the same day: the first, FL10, was carried out in the morning and was interrupted by rain events. The second, FL10, was carried out in the afternoon, after the rain. The differences in coherences of flights FL05-FL10 (Figure 2 middle) and FL05-FL11 (Figure 2 right) reflect the weather conditions causing dielectric changes.

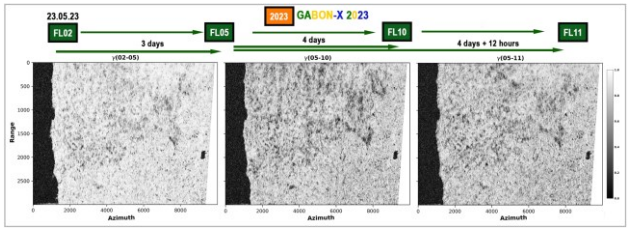

Figure 2: Interferometric coherence for three and four days between three flights of the AfriSAR-2 2023 campaign (from left to right we are the coherences between flights 02 and 05, flights 05 and 10 and between flights 05 and 11).

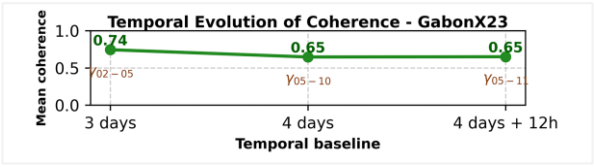

Figure 3: Temporal evolution of the coherence on AfriSAR-2 2023 campaign over the Mondah test site

A general trend is observed, characterized by relative stability between two successive acquisitions with four days temporal baseline. The interferometric coherences between flights FL02 and FL05 (Figure 4 on the left) and FL05 and FL08 (Figure 4 on the right) remain relatively high, with average signal coherence values ranging from 0.77 to 0.76 (Figure 5) for 4 days.

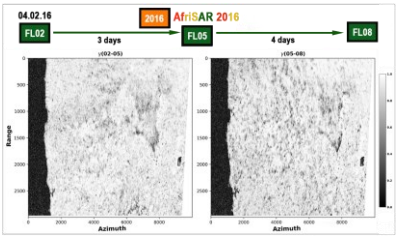

Figure 4: Interferometric coherence for four days between two flights of the AfriSAR-1 2016 campaign (respectively between flights 02 and 05 on left and 05 and 08, on right)

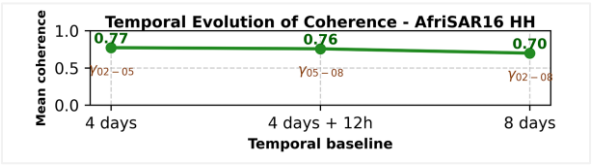

Figure 5: Temporal evolution of the coherence on AfriSAR-1 2016 campaign over Mondah test site for 4 and 8 days

Finally, looking into relatively longer temporal baseline of seven to eight days, we still observe a relatively high coherence, both in 2023 with AfriSAR-2 (Figure 6 on the left and in the middle) and in 2016 with AfriSAR-1 (Figure 6 on the right). The mean values remain relatively high: 0.64 between FL02 and FL10, and 0.67 between FL02 and FL11 (Figure 7).

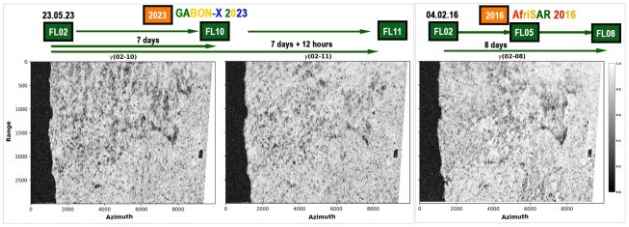

Figure 6: Temporal coherences for around a week. From left to right: coherences FL02-FL10 and FL02-FL11 of the AfriSAR-2 2023 and between the FL02 and FL08 of the AfriSAR-1 2016 campaign.

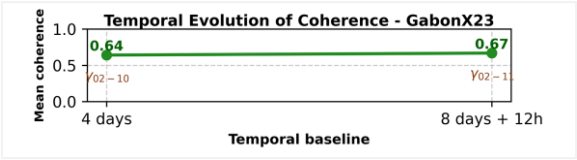

Figure 7: Temporal evolution of the coherence on AfriSAR-2 2023 campaign for 8 days over Mondah test site

The 8 days coherence of AfriSAR-1 is close to those observed with AfriSAR-2, 0.70 (Figure 5) and 0.67 (Figure 7).

4.2 BIOMASS temporal stability

4.1.1 Interferometric coherence behaviour

The interferometric coherence maps (Figure 8) computed using (1) with the different interferometric pairs 09-12, 12-15 and 09-15 generally show relatively overall high values ($\gamma \approx 0.7$-1), with some spatial variability across the scene. Primarily, for the interferometric pair 09-12 (Figure 8, left), separated by three days where the values appear more homogeneous and closer to 1.

The pair 12–15 (3 days, Figure 8, middle), shows a marked contrast with relatively lower values across the entire scene, likely caused by wind or rainfall effects between acquisitions.

The interferometric coherence for 6 days (9-15, Figure 8, right), on the other hand, shows localized coherence losses particularly in structurally heterogeneous forest in the forest zone of Gabon, near La Lopé.

This spatial variability reflects the combined influence of several different types of decorrelation mechanism, notably volumetric and temporal. Therefore, to identify the cause of the presence of low values in the interferometric coherences obtained, the coherence was decomposed as a function of its geometric dependence on the wavenumber (k_z), the modelled volumetric coherence (γ_{vol}) and the temporal coherence (γ_{temp}).

This was achieved by decomposing the interferometric coherence obtained (1) into several of its independent decorrelation contributions, as follows [13], [14]:

$$\tilde{\gamma}(S_1, S_2^*) = \tilde{\gamma}_{vol} * \tilde{\gamma}_{temp} * \tilde{\gamma}_{rg} * \tilde{\gamma}_{sys} \qquad (2)$$

where γ_{rg} denotes the range spectral decorrelation induced by the spatial baseline and γ_{sys} includes the decorrelation induced by the system during acquisition such as additive noise.

4.1.2 Influence of vertical wavenumber

The vertical wavenumber (k_z) is proportional to the difference in viewing angle $\Delta\theta$ between two acquisitions and inversely proportional to the radar wavelength λ and the angle of incidence θ_0 (3).

It represents the sensitivity of the InSAR phase difference to the vertical structure of the features present in the captured scene. It is influenced by the acquisition geometry and is defined by the following formula for the monostatic mode:

$$k_z = \frac{4\pi}{\lambda} \frac{\Delta\theta}{sin\,(\theta_0)} \qquad (3)$$

The distributions of vertical wavenumber in COM-1 phase of BIOMASS mission takes relatively low values (0.005-0.02) (Figure 9 left). Although slight variations are observed, they do not exhibit significant shifts that could explain the observed coherence changes.

This indicates that baseline-dependent geometric effects have a limited impact on the coherence variations. Consequently, k_z is not the primary driver of decorrelation in the COM-1 phase.

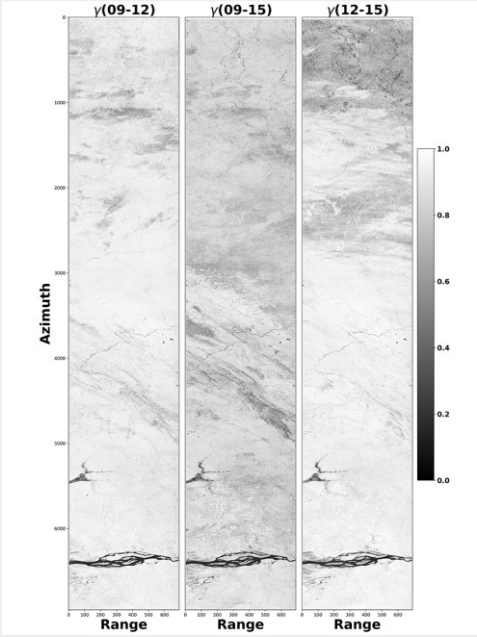

Figure 8: Interferometric coherence maps: two days baseline 09-12 (left) and 12-15 (on the middle) and six days 09-15 (on the right).

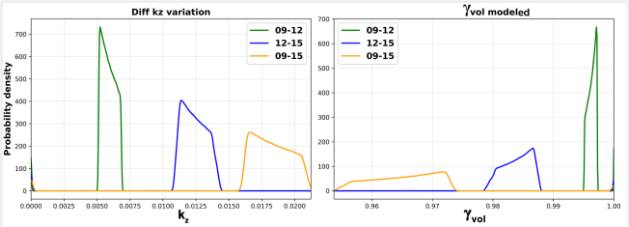

Figure 9: The vertical wavenumber k_z distribution (left) and γ_{vol} distribution (right) for different combinations with the green, blue and yellow respectively 09-12, 12-15 and 09-15 different interferometric pairs.

4.1.3 Volumetric coherence contribution

Volumetric decorrelation, defined in [11] and [12] as the decorrelation induced by the different projection of the vertical component of the scatterers in the two images forming the interferogram, is the component of the interferometric coherence linked to the 3D volume structure of the scatterers present in the image scene.

It's intrinsically linked to the vertical distribution of scatterers by means of the Fourier transform of the vertical reflectivity profile $F(z,\vec{w})$:

$$\tilde{\gamma}_{vol}(k_z,\vec{w}) = e^{j\varphi_0}\frac{\int_0^{h_v} F(z,\vec{w})e^{jk_z z}dz}{\int_0^{h_v} F(z,\vec{w})dz} \qquad (4)$$

with $\vec{w}$ the unitary complex vector related to the choice of polarization and φ_0 represents the ground phase related to the ground elevation z_0 by $\varphi_0 = k_z z_0$. Finally, the $\tilde{\gamma}_{vol}$ was derived as a function of the product of vegetation height (h_v) and the vertical wavenumber (k_z) as following:

$$|\tilde{\gamma}_{vol}(k_z,\vec{w})| = \left|\frac{\sin(\frac{h_v k_z}{2})}{(\frac{h_v k_z}{2})}\right| \qquad (5)$$

The modelled volumetric coherence ($\tilde{\gamma}_{vol}$) obtained using the sinc function (5), considers a constant in height vertical reflectivity profile.
Even if h_v is fixed to a large value of about 50 metres, γ_{vol} still shows consistently high values, ($\gamma_{vol} \approx 0.95$-1) with a narrow distribution with minimal variability across all interferometric pairs (Figure 9 right) 09-12 (right), 12-15 (middle) and 09-15 (left). This behaviour confirms that volumetric decorrelation is low in the BIOMASS COM-1 dataset, due to nominally almost zero spatial baseline.

4.1.4 Temporal decorrelation contribution

Temporal decorrelation describes changes in the scene structure and permittivity conditions between acquisitions and characterized by the loss of coherence between two radar acquisitions [11].

In contrast, the temporal coherence (γ_{temp}) obtained using (6), exhibits a broad distribution, with values ranging approximately from 0.6 to 1, with clear differences between interferometric pairs (Figure 11). The widest distributions and lowest values are observed for the longest temporal baseline (09–15, left), indicating increased decorrelation.

$$\tilde{\gamma}_{temp} = \frac{\tilde{\gamma}_{(S_1S_2)}}{\tilde{\gamma}_{vol}\tilde{\gamma}_{rg}\tilde{\gamma}_{sys}} \qquad (6)$$

With:

$$\tilde{\gamma}_{rg} = 1 - \left|\frac{k_z}{k_z^{Crit}}\right| \qquad (7)$$

where k_z^{Crit} is the critical vertical wavenumber [14]. The spatial patterns of γ_{temp} (Figure 11) closely match those observed in the interferometric coherence maps (Figure 8), confirming that temporal decorrelation is the dominant factor controlling coherence variations. Given that geometric decorrelation contributions remain close to unity and negligible system induced decorrelation, the observed coherence can be finally approximated:

$$\tilde{\gamma}_{(S_1S_2)} \approx \tilde{\gamma}_{temp} \qquad (8)$$

This demonstrates that temporal decorrelation directly governs the interferometric coherence in the COM-1 configuration and it's attributed to short-term environmental dynamics including wind-induced canopy motion, moisture variations or vegetation dynamics.

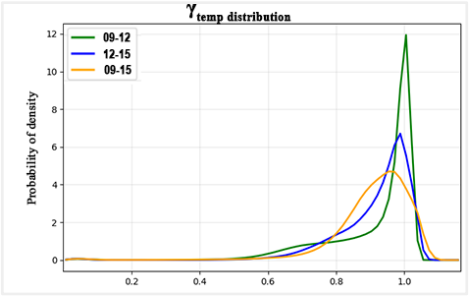

Figure 10: The γ_{temp} distribution for different combinations with the green, blue and yellow respectively 09-12, 12-15 and 09-15 different interferometric pairs.

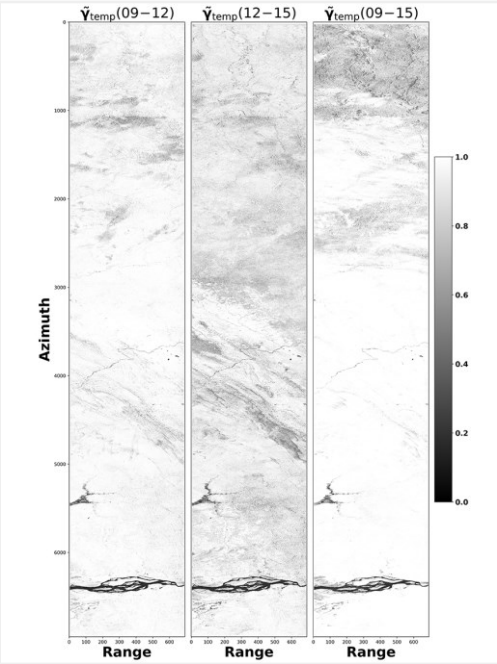

Figure 11: Temporal decorrelation maps: two days baseline 09-12 (left) and 12-15 (on the middle) and six days 09-15 (on the right)

The COM-1 analysis shows that volumetric coherence γ_{vol} remains close to 1, while temporal decorrelation γ_{temp} accounts for most of the observed variability. As a result, interferometric coherence is mainly controlled by temporal effects, which should be accounted when retrieving forest structure parameters in tropical environments.

4.2 Comparative analysis

A comparative analysis of P-band SAR interferometric coherence acquired 9 days apart from the BIOMASS mission and airborne AfriSAR-3 campaign is conducted for La Lopé, Gabon (red box, Figure 12). The results show that both products exhibit relatively high overall coherence values across the scene ($\gamma \approx 0.5$-1) (Figure 12).

The interferometric coherences of BIOMASS for 3, 6 and 9 days were compared with those of the AfriSAR-3 2025 campaign as a reference.

- 3 days: A high concentration of coherence values in the interval [0.85 - 1.0] with a BIOMASS distribution slightly more spread out than F-SAR and a slightly less pronounced coherence peak, signifying good overall coherence. BIOMASS correctly reproduces high levels.

- 6 days: relatively more marked deviations are observed with the appearance of a tail of distribution towards low coherences ($\gamma \approx 0.3$-0.7) with a reduction in the main peak compared with F-SAR and an overall shift towards lower values implying that BIOMASS has slightly more decorrelation.

- 9 days: Shows better agreement with F-SAR than the 3- and 6-days cases with well aligned coherence peaks. However, the BIOMASS distribution is wider, with the persistent presence of weaker coherences, as evidenced by the appearance of a distribution tail towards the weak coherences ($\gamma \approx 0.2$-0.7).

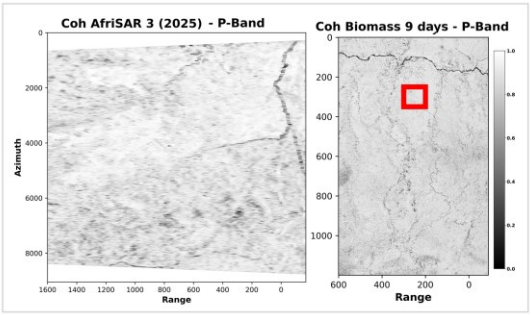

Figure 12: Interferometric coherence maps at 9 baseline days for AfriSAR-3 2025 (left) and BIOMASS (right) data over La Lopé, with the common area indicated by red box.

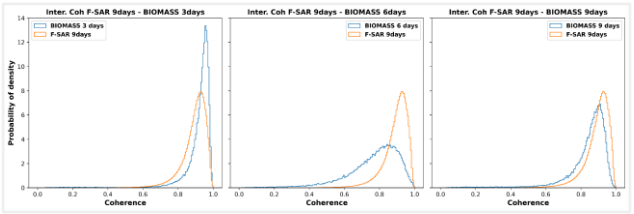

Figure 13: Probability distributions of interferometric coherence for three cases: from left to right: BIOMASS 3 days, 6 days and 9 days (blue) vs F-SAR 9 days (orange).

Overall, both distributions are highly concentrated towards high coherences ($\gamma \approx 0.7$-0.95), implying that the La Lopé forest exhibits generally high radar stability in the P-band due to persistent dominant mechanisms (trunks, deep volume). Despite its much finer F-SAR resolution, BIOMASS nevertheless maintains high P-band coherence over dense forests.

5 Conclusion

This study examines the temporal stability of P-band interferometric coherence in tropical forests in the context of the BIOMASS in orbit commissioning phase, combining COM-1 data analysis and comparison with AfriSAR-3 2025 (F-SAR) airborne data.

An overall high temporal coherence in BIOMASS interferometric acquisitions, with values comparable to those obtained by airborne campaigns. However, strong temporal decorrelation patterns emerge, driven by weather effects such as rainfalls affecting the dielectric properties of the reflectivity volume.

These low temporal coherence patterns may introduce biases in the retrieval of forest structural parameters such as height and above-ground biomass if not accounted. These results highlight the critical need to accurately model temporal decorrelation in P-band interferometric processing chains in order to ensure the reliable large-scale forest monitoring.

6 Literature

[1] Boucka, F., Obame, C., Manfoumbi, F., Mba, A., Ondo, M., Ovono, V., & Ndjoungui, A. (2021). Cartographie de l'occupation du sol du Gabon en 2015 : Changements entre 2010 et 2015. *Revue Française de Photogrammétrie et de Télédétection, 223*, 118–128. doi.org/10.52638/rfpt.2021.567

[2] Choi, C., Pardini, M., Heym, M., & Papathanassiou, K. P. (2021). Improving forest height-to-biomass allometry with structure information: A Tandem-X study. *IEEE Journal of Selected Topics in Applied Earth Observations and Remote Sensing, 14*, 10415–10427. doi.org/10.1109/JSTARS.2021.3116443

[3] Okanga-Guay, M., Ondo Assoumou, E., Akendengue Aken, I., Mpie Simba, C., & Mombo, J.-B. (2019, March). Suivi des changements spatiaux et environnementaux dans les mangroves de la province de l'Estuaire du Gabon. In *Conférence OSFACO : Des images satellites pour la gestion durable des territoires en Afrique* (Cotonou, Bénin).

[4] Saatchi, S. S., Harris, N. L., Brown, S., Lefsky, M., Mitchard, E. T. A., Salas, W., Zutta, B. R., Buermann, W., Lewis, S. L., Hagen, S., Petrova, S., White, L., Silman, M., & Morel, A. (2011). Benchmark map of forest carbon stocks in tropical regions across three continents. *Proceedings of the National Academy of Sciences, 108*(24), 9899–9904. doi.org/10.1073/pnas.1019576108

[5] Pardini, M., Tello, M., Cazcarra-Bes, V., Papathanassiou, K. P., & Hajnsek, I. (2018). L- and P-band 3-D SAR reflectivity profiles versus lidar waveforms: The AfriSAR case. *IEEE Journal of Selected Topics in Applied Earth Observations and Remote Sensing, 11*(10), 3386–3401.

[6] Hajnsek, I. "Technical assistance for the development of airborne SAR and geophysical measurements during the AfriSAR campaign," ESA : Paris, France, Final Tech. Rep. 4000114293/15/NL/CT, 2011.

[7] Fatoyinbo, L., Armston, J., Simard, M., Saatchi, S., Denbina, M., Lavalle, M., Hofton, M., Pinto, N., Hancock, S., Tang, H., Marselis, S., Hawkins, B., Duncanson, L., Blair, B., Hansen, C., Lou, Y., Dubayah, R., Hensley, S., Silva, C., Poulsen, J., Labrière, N., Barbier, N., Jeffery, K., Kenfack, D., Alonso, A., Moussavou, G., Lewis, S., & Hibbard, K. (2021). The NASA AfriSAR campaign: Airborne SAR and lidar measurements of tropical forest structure and biomass in support of future space missions. *Remote Sensing of Environment, 264*, 112533.

[8] Labrière, N., et al. (2018). In situ reference datasets from the TropiSAR and AfriSAR campaigns in support of upcoming spaceborne biomass missions. *IEEE Journal of Selected Topics in Applied Earth Observations and Remote Sensing, 11*(10), 3617–3627. doi.org/10.1109/JSTARS.2018.2851606

[9] Marselis, S. M., Tang, H., Armston, J. D., Calders, K., Labrière, N., & Dubayah, R. (2018). Distinguishing vegetation types with airborne waveform LiDAR data in a tropical forest–savanna mosaic: A case study in Lopé National Park, Gabon. *Remote Sensing of Environment, 216*, 626–634.

[10] Mitchard, E. T. A., Saatchi, S. S., White, L. J. T., Abernethy, K. A., Jeffery, K. J., Lewis, S. L., Collins, M., Lefsky, M. A., Leal, M. E., Woodhouse, I. H., & Meir, P. (2012). Mapping tropical forest biomass with radar and spaceborne LiDAR in Lopé National Park, Gabon: Overcoming problems of high biomass and persistent cloud. *Biogeosciences, 9*(1), 179–191.

[11] Moreira, A., Prats-Iraola, P., Younis, M., Krieger, G., Hajnsek, I., & Papathanassiou, K. (2013). A tutorial on synthetic aperture radar. *IEEE Geoscience and Remote Sensing Magazine, 1*, 6–43. doi.org/10.1109/MGRS.2013.2248301

[12] Hajnsek, I., Kugler, F., Lee, S.-K., & Papathanassiou, K. (2009). Tropical-forest-parameter estimation by means of Pol-InSAR: The INDREX-II campaign. *IEEE Transactions on Geoscience and Remote Sensing, 47*, 481–493. doi.org/10.1109/TGRS.2008.2009437

[13] Askne, J., Dammert, P., Ulander, L. M. H., & Smith, G. (1997). C-band repeat-pass interferometric SAR observations of the forest. *IEEE Transactions on Geoscience and Remote Sensing, 35*, 25–35. doi.org/10.1109/36.551931

[14] Guliaev, R., Kim, J. S., Pardini, M., & Papathanassiou, K. P. (2024). On the use of tomographically derived reflectivity profiles for Pol-InSAR forest height inversion in the context of the BIOMASS mission. *IEEE Transactions on Geoscience and Remote Sensing, 62*, 1–12. doi.org/10.1109/TGRS.2024.3497572